

## A quantitative study of the 6NM-64 neutron monitor by using Geant4: 1. Detection efficiency for different particles



P. Paschalis<sup>a</sup>, H. Mavromichalaki<sup>a,\*</sup>, L.I. Dorman<sup>b,c</sup>

<sup>a</sup> Nuclear and Particle Physics Section, Physics Department, National and Kapodistrian University of Athens, Zografos 15783, Athens, Greece

<sup>b</sup> Israel Cosmic Ray & Space Weather Centre and Emilio Segrè Observatory, Affiliated to Tel Aviv University, Golan Research Institute, and Israel Space Agency, Qazrin 12900, Israel

<sup>c</sup> Cosmic Ray Department of N.V. Pushkov IZMIRAN, Russian Academy of Science, Troitsk 142190, Moscow, Russia

### ARTICLE INFO

#### Article history:

Received 5 June 2013

Received in revised form

27 July 2013

Accepted 17 August 2013

Available online 30 August 2013

#### Keywords:

Cosmic rays

Neutron monitors

Geant4

Simulation

Detection efficiency

### ABSTRACT

The neutron monitors are the ground based detectors that continuously measure the flow of the cosmic rays that reach the earth's surface. The measurements of the neutron monitors are of great importance for the scientific community since they contribute to the study of several scientific fields, such as the solar activity and the prediction of the space weather. For this reason, most of the neutron monitors worldwide are organized in a network, in order for their measurements to be easily accessible. The correct evaluation of the measurements and their connection with the physical quantities of the cosmic rays require the knowledge of the interactions and the detection procedure that take place inside the neutron monitor. In this work a quantitative study of the 6NM-64 behavior is presented based on Monte Carlo simulations by using the well known Geant4 simulations toolkit. The study focuses on the detection efficiency of the neutron monitor, both in sections and as a whole for the different particle species, on its dependence on the incident direction of the particles and on the secondary neutrons produced inside the neutron monitor.

© 2013 Elsevier B.V. All rights reserved.

### 1. Introduction

The cosmic rays are high energetic particles, mainly protons, alpha particles and heavier nuclei that originate from galactic and stellar sources. The cosmic rays, modulated and in some cases enhanced by the solar activity, penetrate the Earth's magnetic field and reach the atmosphere. The nuclear interactions of these particles with the molecules of the atmosphere produce cascades of secondary particles, finally consisting of muons, neutrinos, electrons, positrons, gamma and the hadronic component which means neutrons, protons,  $\pi^\pm$  and  $K^\pm$ . These particles can reach the Earth's surface and be detected by ground based detectors.

The neutron monitor is a ground based detector that continuously measures the flow of the hadronic component of the secondary cosmic rays. It was invented by J.A. Simpson who also developed the first standardized type of neutron monitor, known as IGY type [1]. Later, a new and optimized neutron monitor was developed and standardized by Carmichael, known as NM64 or supermonitor [2,3]. Both of these neutron monitors use similar architecture consisting of proportional counters filled with  $\text{BF}_3$  gas. Due to the great lifetime of the counters, neutron monitors of

these types are still being fully operated with some modifications in the electronics and the data acquisition systems [4]. Nowadays, many types of neutron monitors have been developed, most of which use proportional counters filled with  $^3\text{He}$  [5–8]. However, proportional counters with  $\text{BF}_3$  are still constructed and used in some new types of neutron monitors. The great importance of monitoring the cosmic ray flux in different latitudes has led to the creation of the worldwide network of neutron monitors, where several stations participate regardless of the neutron monitor type they host. The cosmic ray flux is measured through the hadronic component and the scientists evaluate changes in the cosmic ray flux in respect to the latitude of the station. In this task contributes the recent development of the Neutron Monitor Database (<http://www.nmdb.eu>) where the stations can send their high resolution measurements in real time [9,10].

All the types of neutron monitors share the same architecture. Each counter is positioned inside a cylindrical volume, the moderator, which is made of a material with low molecular mass. The moderator is positioned inside another cylindrical volume, the producer, which is made of a material with high molecular mass. The whole system is surrounded by a rectangular volume, the reflector, which is made of a low molecular mass material. The low molecular mass material is paraffin for the IGY neutron monitor, low density polyethylene for the NM64 and high density polyethylene for the new types of neutron monitor that use  $^3\text{He}$  gas.

\* Corresponding author. Tel.: +302107276890.

E-mail address: [emavromi@phys.uoa.gr](mailto:emavromi@phys.uoa.gr) (H. Mavromichalaki).

The high molecular mass material is high purity lead in all cases. In the detection procedure, the reflector prevents the thermal neutron from entering the detector. The particles that pass through the reflector, interact with the lead nucleus of the producer and secondary neutrons are produced via the inelastic scattering. The secondary neutrons slow down through the elastic scattering in the moderator, are reflected through the elastic scattering in the reflector and produce new secondary neutrons through additional inelastic scatterings in the lead. The result of these procedures is the generation of a great number of secondary neutrons that are gradually slowed down to thermal energies. At thermal energies, the cross-section of neutron capture from Boron-10 or Helium-3 inside the counters is significant. The neutron capture from Boron-10 produces an alpha particle via the interaction  $^{10}\text{B}(n,\alpha)^7\text{Li}$  with energy 1.47 MeV (93.7% probability) or 1.78 MeV (6.3% probability) while the capture from Helium-3 produces a proton with 573 keV energy via the interaction  $^3\text{He}(n,p)^3\text{H}$ . The generation of the alpha particle or the proton into the counter produces a pulse according to the operational principle of proportional counters [11].

The quantification of the processes that happen inside the neutron monitor is essential in order to connect the measurements with the changes of the cosmic ray flux. The optimal method to perform such quantifications is through simulations. Such simulations have been performed in the past [12] by using the FLUKA simulation package. In this work, a simulation of the 6NM-64 neutron monitor, like the one used in the Athens Station [13,14], (<http://cosray.phys.uoa.gr>), is performed by using the Geant4 simulation toolkit [15,16]. Geant4 is a well known simulation package, written in C++, that was initially developed for the simulation of high energy physics and gradually got enhanced in order to be applied to lower energies [17–20]. The package provides a huge variety of options and great support through the official and unofficial web communities (<http://geant4.cern.ch>). For all these reasons Geant4 is currently used for a variety of applications such as high energies, nuclear physics and medical physics. In the field of cosmic rays research, Geant4 has also been used. Planetocosmics [21] and Magnetocosmics [22] are applications of Geant4. The Plateau de Bure Station group used the Geant4 in order to simulate the operation of the  $^3\text{He}$  neutron monitor that they had installed [8]. Finally, Balabin et al. [23] and Mauricev et al. [24] used the Geant4 in order to examine the multiplicity and some parameters of the neutron monitor respectively. In this work, a complete simulation of the 6NM-64 neutron monitor is presented that leads to the calculation of several parameters. More specifically, the detection efficiency for the

different particle species and for a wide range of energy, its dependence on the incident direction and the surface section of the neutron monitor in which the incident occurs, the number of the secondary neutrons in the neutron monitor and finally their energy spectrum are studied.

## 2. Application setup

The Geant4 package is a C++ toolkit which, as its name declares (GEometry ANd Tracking), provides an efficient way to track particles that interact with materials distributed in a volume. The package is fully modulated and provides a variety of base classes that the user should use in order to develop his own classes by using the C++ inheritance feature. A Geant4 application is fully controlled by the G4RunManager class in which the user passes the pointers of the objects that are used in the simulation and by the G4UImanager class in which the user passes the necessary for the application commands. This sophisticated approach optimizes the whole procedure and reduces the hazard of memory leaks. A Geant4 application requires at least the objects of three classes that respectively configure the geometry (G4VUserDetectorConstruction), the particle beam (G4VPrimaryGeneratorAction) and the physical interactions (G4VUserPhysicsLists) that will be taken into account during the simulation. Apart from these mandatory classes, there are some optional classes (G4UserRunAction, G4UserEventAction, G4UserStackingAction, G4UserTrackingAction, G4UserSteppingAction) that the user can define and that are invoked by the G4RunManager during the simulation procedure. These classes allow access to parameters and variables and can be used in order to obtain information about the simulation process, such as the creation of new particles, their position and their energy. In practice, the necessary information can be obtained in several ways and the user should develop the most optimal and efficient one, according to the parameters that will be measured. Finally, an important feature of the package is the provision of several visualization drivers via the G4VisManager class which are very useful for the verification of the correct geometry and for the depiction of the simulation.

The structure of the application developed in this work is illustrated in Fig. 1. The application allows the user to define parameters about the beam, the position of the neutron monitor and the physics list. Apart from the mandatory classes, it uses a G4UserStackingAction class in order to obtain the results of the simulation. The results are stored in csv files for later processing.

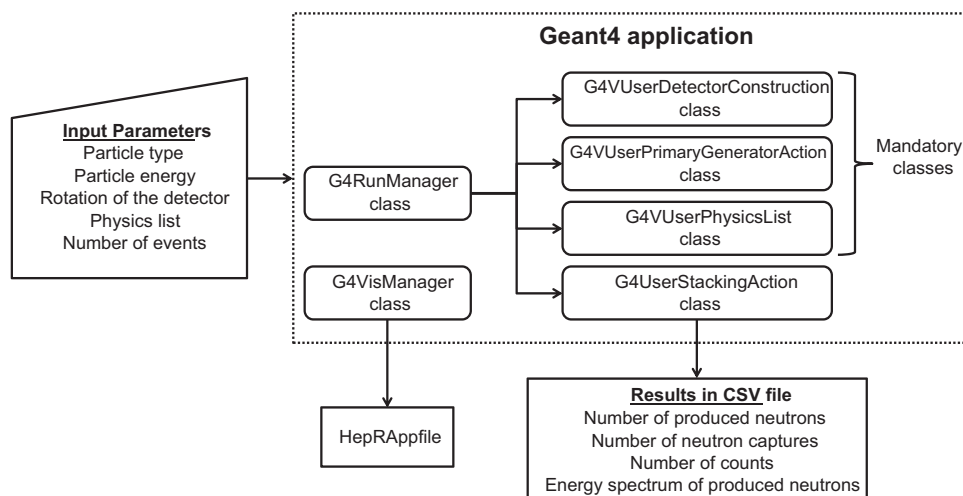


Fig. 1. Structure of the Geant4 application.

Finally, the application supports the visualization of a run through the HepRApp driver. A more thorough description of the application is given in the following paragraphs.

The geometry that is defined in the G4VUserDetectorConstruction object is the 6NM-64 neutron monitor as illustrated in Fig. 2. The components and the dimensions of the geometry are accurately defined according to Carmichael [2]. The neutron monitor consists of 6 proportional counters with 14.85 cm internal diameter and 190.8 cm length. The counters are constructed of stainless steel with 0.8 mm thickness and are filled with BF<sub>3</sub> gas in 20 cm Hg pressure. The Boron element is enriched in order to consist of 96% <sup>10</sup>B and 4% <sup>11</sup>B. Each counter is surrounded by the polyethylene moderator with 2 cm thickness and the lead producer in the shape that is illustrated in the figure. Each producer is supported by aluminum supporting channels. The center of each counter has a 50 cm distance from the neighboring counters and the whole system is surrounded by a polyethylene reflector box that has 7.5 cm thickness. The neutron monitor is laying on the X–Z plane and the counters are parallel to the Z axis. However, the application allows the user to induce a rotation of the neutron monitor around the Z or X axis. The world volume where the neutron monitor is positioned is filled with an extremely low

pressure gas, simulating vacuum, in order to avoid interactions of particles outside the neutron monitor.

The particle beam is defined in the G4VPrimaryGeneratorAction object and consists of monoenergetic particles of the same type and with parallel tracks. The type and the number of particles, the distance between them and the width of the beam are defined by the user. In this work, beams consisting of neutron, protons, pi<sup>+</sup>, pi<sup>-</sup>, mu<sup>+</sup> and mu<sup>-</sup> and with energies from a few eV to 100 GeV were used. The beam is always perpendicular to the X–Z plane where the neutron monitor is laying. It is important to notice that every particle of the beam is handled by the application as a different event. About the physics list used by the application, several cases were evaluated in order to conclude which is the optimal one. A complete description is presented in Section 3.

The results of the simulation are obtained by using a G4UserStackingAction class which is invoked by the G4RunManager every time a new particle is created. Information such as the energy and the momentum of the new particle, the physical volume where it is created, the creation time and its parent particle are available through this class. In this work, the G4UserStackingAction is developed in a way where for a whole run, the measured

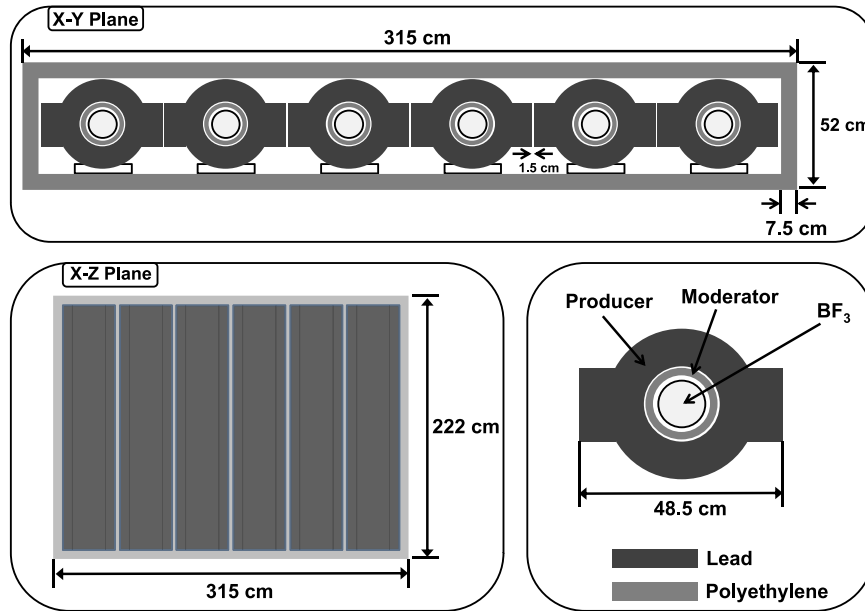


Fig. 2. Construction diagram of the 6NM-64.

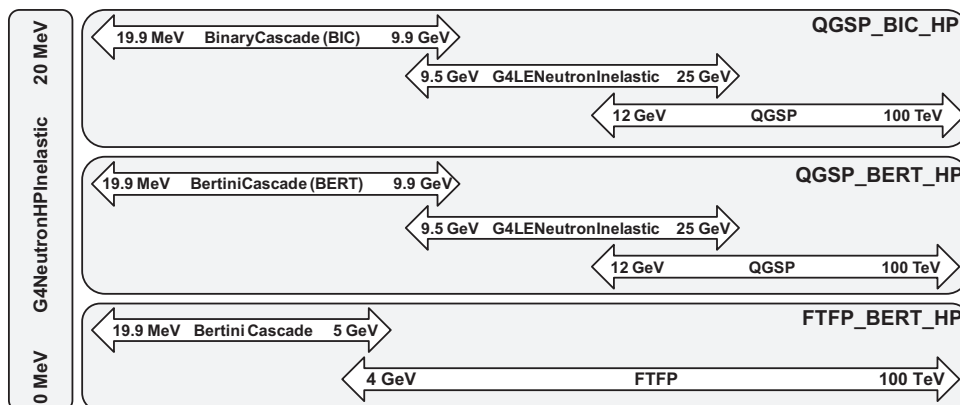


Fig. 3. Geant4 physics models for neutron inelastic scattering.

quantities are the total number of the produced neutrons in the neutron monitor, their energy, the number of neutron captures in the  $^{10}\text{B}$  and the number of the registered counts. The results, accompanied with information about the run, are stored in csv files for later processing. From the development point of view, the total number of neutrons and their energy can be easily obtained just by checking if a newly created particle is neutron or not and by recording its energy. In order to measure the neutron captures in the counters, the fact that a neutron capture from  $^{10}\text{B}$  results in the generation of an alpha particle with energies 1.47 MeV and 1.78 MeV is used. In the application, every generation of an alpha particle with these two energies in the physical volumes of the  $\text{BF}_3$  gas is considered as a neutron capture. Finally, the measurement of

the counts is a more complicated procedure. The global time of each neutron capture in  $\text{BF}_3$  is registered and then the total number of counts is calculated, considering that each counter has about  $5\ \mu\text{s}$  recovery time and the electronics of the neutron monitor  $20\ \mu\text{s}$  dead time.

The application is using Geant4.9.6 installed on a machine running debian linux. In order to obtain the required accuracy of the results and to calculate the errors, several runs were performed for every case. The seed of the random generator used by the application was randomized at the beginning of each run. The results presented in this work required months of runs. In order to reduce the required time, batch files containing several runs were distributed to several computers.

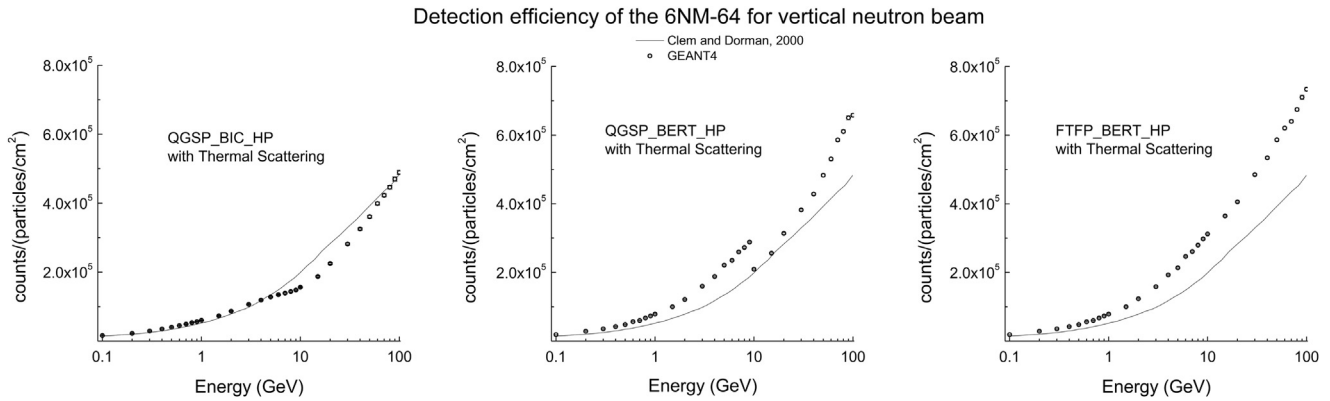


Fig. 4. Comparison of the Geant4 physics lists based on the detection efficiency of neutrons.

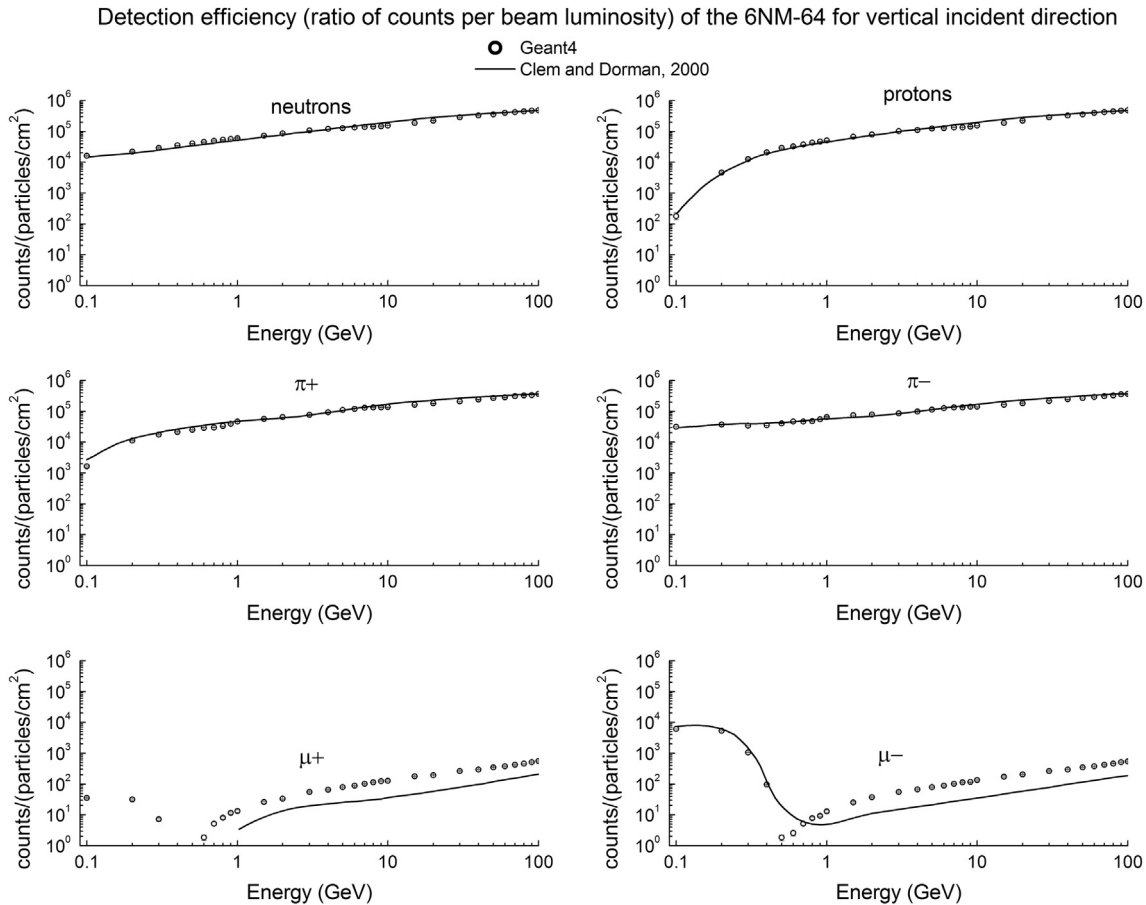


Fig. 5. Detection efficiency of the 6NM-64 for vertical beam.

### 3. Selection of the physics list

The most critical part of the simulation setup is the selection of the physics list which contains the available interactions for the simulation. Geant4 provides several models for each interaction and each one works in a specific energy range. The toolkit allows the user to select the most appropriate models which can be a very challenging task. However, Geant4 provides some predefined physics lists that have been constructed through the experience and the validation of past applications and experiments. In order to build the appropriate physics list or to use one of the predefined ones, it is important to consider the physical procedures that take place from the time that a particle enters the neutron monitor to the time a count is registered. As it has been described in the introduction, the operation of the neutron monitor is dominated by the generation of the secondary neutrons via the inelastic scattering in the lead nucleus. The neutrons gradually slow down to thermal energies where the cross-section of capture from  $^{10}\text{B}$  into the counters is significant. As a result, the simulation is very sensitive to the accurate handling of neutrons in low energies and to the accurate simulation of hadrons inelastic scattering.

Regarding the handling of neutrons in low energies, Geant4 provides high precision datasets for neutrons from 0 MeV to 20 MeV by using the NeutronHP model. Regarding the inelastic scattering of hadrons, several models exist depending on the energy range. The most common models that Geant4 provides for the inelastic scattering of hadrons are the Binary Cascade model for energies up to 10 GeV (1.3 GeV for pions), the Bertini Cascade model for energies up to 10 GeV, the LEP model for energies up to 25 GeV, the FTFP model for energies from 3 GeV to 100 TeV and the QGSP model for energies from 12 GeV to 100 TeV. The matching of these models in order to cover the energy range from 0 to several GeV is not a straight forward procedure. In this work several physics lists were tested in order to conclude which one is the most appropriate for the processes inside the neutron monitor. The base of these tests where the QGSP\_BIC\_HP, QGSP\_BERT\_HP and the FTFP\_BERT\_HP physics lists. The models that these physics lists use for the inelastic scattering of hadrons are presented in Fig. 3. These physics lists have also been used in the past for the simulation of neutron monitors. The base for the simulation of Semikh et al. [8] was the QGSP\_BIC\_HP while Maurchev et al. [24] used the QGSP\_BERT\_HP physics list. In accordance to [8], the physics lists that have been tested and used in this work have been modified in order to include the thermal scattering of neutrons in polyethylene and the G4MuonNucleusProcess for the interactions of muons with nucleus.

The selection of the physics list is made by calculating the detection efficiency of the 6NM-64 for a vertical neutron beam and comparing the obtained results with the ones calculated by Clem and Dorman [12] who had used the FLUKA toolkit. As the authors of this work described, the neutron monitor is fully illuminated with a beam of monoenergetic particles in the vertical direction and the registered counts are measured. The results of Geant4 for a neutron beam compared to the results of Clem and Dorman [12] are presented in Fig. 4. In this figure, the FLUKA results should be considered as an approximation, since they have been digitized from the plot presented in Clem and Dorman where a logarithmic scale was used.

As expected, the results of Fig. 4 show how sensitive the simulation of the neutron monitor is on the different handling of the inelastic scattering. The QGSP\_BIC\_HP seems to give identical results with FLUKA up to 5 GeV and from 70 GeV to 100 GeV. From 6 GeV to 60 GeV the calculated detection efficiency seems to be less than the one calculated with FLUKA. A completely different and strange behavior is noticed in the case of QGSP\_BERT\_HP. The calculated efficiency is greater than FLUKA and also there is a

discontinuity at 10 GeV where the Bertini Cascades model is changed to LEP. In the FTFP\_BERT\_HP case, this discontinuity disappears, however, the calculated efficiency is much greater than the one calculated with FLUKA, in the whole energy range. Based on these results, many other cases were tested in which the shift energy point from Binary and Bertini Cascades to the LEP model was changed in QGSP\_BIC\_HP and QGSP\_BERT\_HP physics list respectively. Tests have also been made with physics lists where the Binary Cascades are combined with the FTFP model. None of these combinations gave a result more similar to FLUKA than the QGSP\_BIC\_HP physics list. These tests and the fact that the same physics list was successfully used by Semikh et al. [8], made QGSP\_BIC\_HP the most appropriate physics list for the simulation of the 6NM-64. In the results presented in this work the G4NDL4.2 dataset was used by the NeutronHP model.

It should be highlighted that the selection of the QGSP\_BIC\_HP physics list for the simulation of the 6NM-64 does not correspond to an evaluation or validation of the Geant4 interaction models. An evaluation procedure requires a comparison between experimental data and the results of the Geant4 simulation which is not in the scope of this work. However, the results of Clem and Dorman [12] agree with the results measured by Shibata et al. [25], who used an accelerator neutron beam in order to measure the detection efficiency of the 6NM-64 for incident neutrons of a few hundred MeV. In any case, since the pattern of the curves is the same for all the physics lists that were tested, the systematic

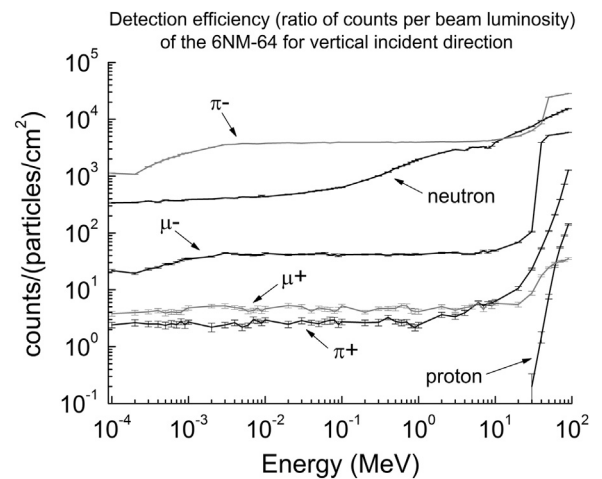


Fig. 6. Detection efficiency of the 6NM-64 for low energy vertical beam.

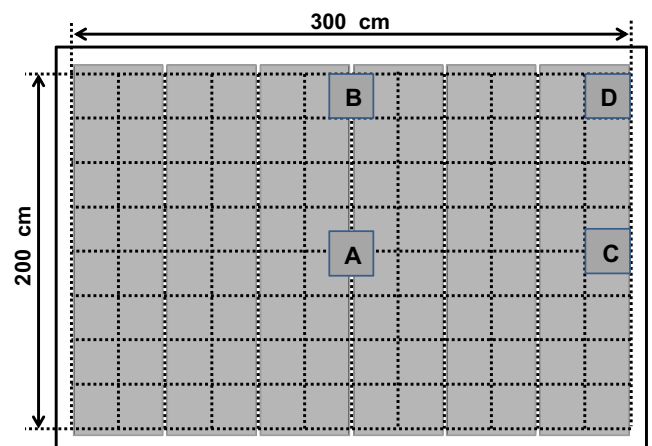


Fig. 7. Division of the neutron monitor surface for the per section calculation of detection efficiency.

errors that the selection of the physics list induces do not affect the conclusions presented below, but differentiate slightly and by the same factor for all the particles species, the calculated values.

#### 4. Detection efficiency of the 6NM-64

The first task of this work is the determination of the detection efficiency of the 6NM-64 for the different particle species. These calculations are important since the secondary cosmic rays that reach the earth's surface consist of many different type of particles. In order to calculate the detection efficiency, the procedure described in [12] is followed, as it has already been mentioned in the previous section. According to this procedure, a parallel beam of monoenergetic particles of the same type fully illuminates the neutron monitor in the vertical direction and the total counts are measured. Simulations are performed for neutron, proton,  $\pi^\pm$ ,  $\mu^\pm$  beams and for an energy range from 100 eV to

100 GeV. For energies above 100 MeV, the beam originates 2 m above the neutron monitor. However, in the low energy range of 100 eV to 100 MeV the beam originates just above the neutron monitor in order to avoid decay phenomena of  $\pi^\pm$ ,  $\mu^\pm$ . Interactions of particles outside the neutron monitor are absent due to the vacuum around it.

The results for the energy range from 100 MeV to 100 GeV are presented in Fig. 5. The detection efficiency is expressed in total counts of the 6NM-64 per beam luminosity (counts/(particles/cm<sup>2</sup>)). For every particle type and for every energy value, the simulation was performed 20 times in order to achieve the required statistical accuracy and to calculate the errors. For the case of  $\mu^\pm$ , the number of repetitions was greater due to the low counting rate. At each plot, the results of Clem and Dorman [12] are presented for comparison reasons. A first conclusion is that Geant4 and FLUKA lead to similar results, which verifies that the selection of QGSP\_BIC\_HP with the thermal scattering enabled and the addition of G4MuonNucleusProcess is an optimal choice for the physics list. Some differences are

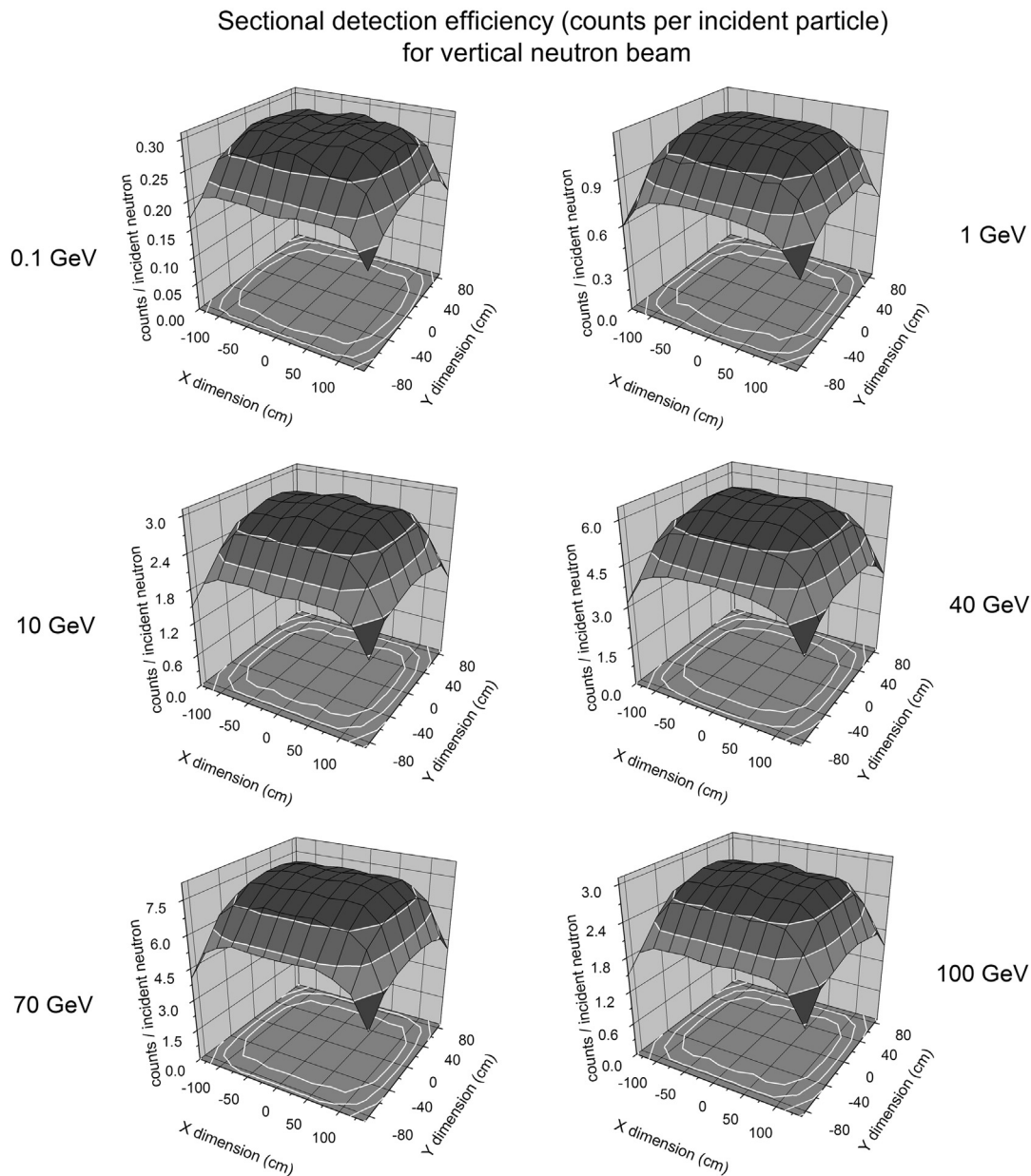


Fig. 8. Per section detection efficiency of the 6NM-64 for vertical neutron beam and several energies.

noticed in muons above 1 GeV but they are not significant. Regarding the results themselves, the conclusions are the same as the ones by Clem and Dorman. More specifically, the detection efficiency in general is significant for neutrons, protons and  $\pi^\pm$  and substantial for  $\mu^\pm$ . The protons and neutrons present identical response for energies above 1 GeV. Below this point, the energy loss of protons, due to ionization, is significant and the detection efficiency for them is much smaller. Negative and positive pions also present an identical response above 1 GeV, but a little less than protons and neutrons due to the smaller cross-section for inelastic scattering. Below 1 GeV, negative pions are captured by lead nucleus and neutrons are produced. As a result, their detection efficiency is greater than the one of positive pions. Finally, the detection efficiency of muons is orders of magnitude less than the one of hadrons. An exception is the behavior of the negative muons at energies below 300 MeV where, like in the negative pions case, their capture from lead nucleus is significant and neutrons are emitted.

The same simulations were performed for the energy range from 100 eV to 100 MeV. At this energy range and due to the lower counting rate, each particle type and each energy value was simulated more than 40 times, in order to achieve the required statistical accuracy. The results are presented in Fig. 6. At this energy range many neutrons cannot penetrate the reflector due to the elastic scattering. As the energy increases, more neutrons penetrate the reflector and as a result the detection efficiency presents a smooth increase. The protons on the other hand, are not detected at all up to 30 MeV. The reason for this is the energy loss due to ionization which prevents them from passing through the reflector. However, above 30 MeV many protons succeed in passing the reflector and the detection efficiency increases rapidly. Regarding the muons, a change in the detection efficiency is noticed at 50 MeV. Up to this energy value negative muons lose their energy due to ionization and are captured in the reflector while positive muons decay inside the reflector. Above this energy

value, the negative muons penetrate the reflector and are captured by the lead nucleus of the producer while the positive muons decay inside the producer. Finally, referring to the pions, a change is also notice at 50 MeV. Up to this energy, positive pions lose their energy inside the reflector and decay to positive muons. The negative pions lose their energy and are captured in the reflector producing, among other particles, neutrons. For this reason, the detection efficiency of negative pions is greater than that of the other particle species. Above 50 MeV, the negative pions reach and interact with the lead nucleus of the producer, while the positive pions decay inside the producer. From the analysis above, it is noticed that the detection efficiency in this energy range, highly depends on the thickness and the density of the reflector.

### 5. Detection efficiency dependence on the NM surface section and on the particle incident direction

After the detection efficiency was determined for the different particle species, a study was made in order to calculate how this efficiency is distributed in the different surface sections of the neutron monitor. The methodology was to divide the surface of the neutron monitor in squares with  $25 \times 25$  cm dimension, as illustrated in Fig. 7, and to measure the detection efficiency if only one square at a time is illuminated with particles. Due to the symmetry, only one quarter of the 96 squares was illuminated. The simulation was performed for vertical neutron beams with energies 0.1 GeV, 1 GeV, 10 GeV, 40 GeV, 70 GeV and 100 GeV. The results in a form of a 3D surface plot are presented in Fig. 8. The plots show the mean counts per incident particle in the specific section of the neutron monitor. For better visualization a contour has been added in the bottom plane of each plot. Two conclusions come out from the results. The first one is that the form of each plot is identical regardless the energy of the particles. The only

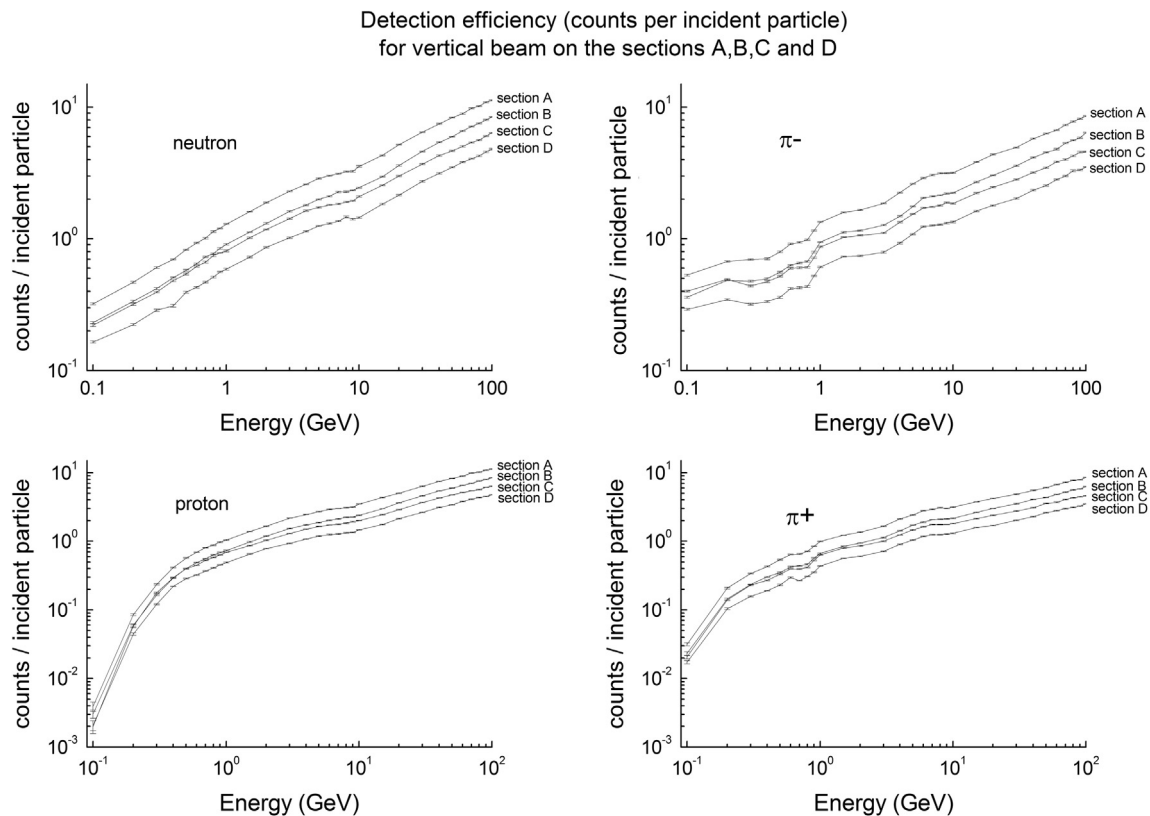
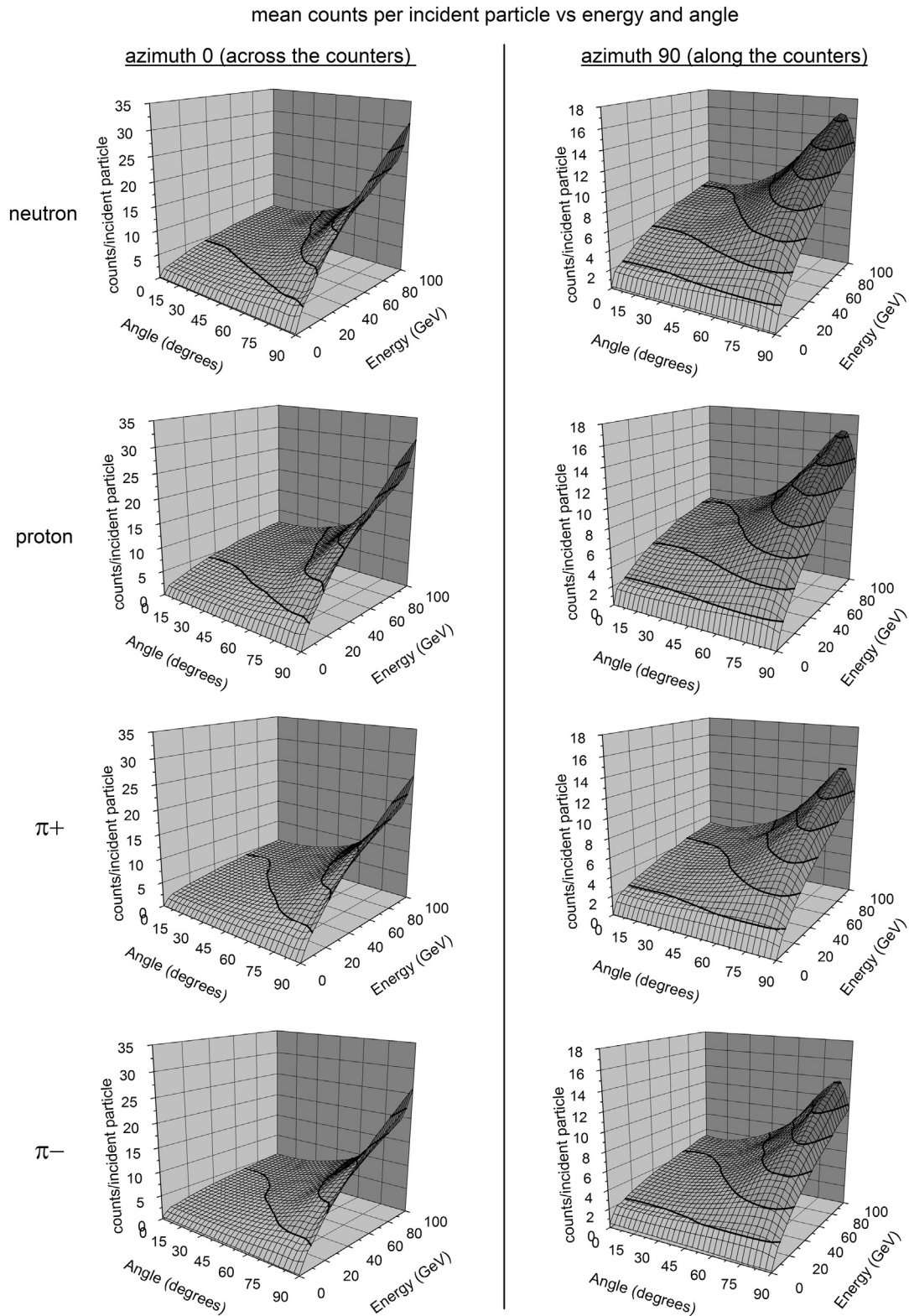


Fig. 9. Detection efficiency for vertical beam on the regions A–D of the neutron monitor.



**Fig. 10.** Detection efficiency as a function of beam angle. The azimuth 0 corresponds to beam angle across the counters while the azimuth 90 corresponds to beam angle along the counters.

change is the expected increase of the counts with the energy increase. The second conclusion is that, as the contour plot shows, the detection efficiency of the neutron monitor is significant and without great changes for a central area with about  $220 \times 120$  cm

dimension. Outside this area the detection efficiency decreases gradually until the edge of the neutron monitor's surface.

Following the conclusions mentioned above, four  $25 \times 25$  cm sections were defined on the surface of the neutron monitor, as

illustrated in Fig. 7. Section A was positioned in the center of the neutron monitor where the greater efficiency is noticed. The 3 remaining sections were positioned on the edge of the neutron monitor's surface, taking into account the symmetry of it. Each section was illuminated with neutrons, protons and  $\pi^\pm$  with energies from 100 MeV to 100 GeV. The results are presented in Fig. 9. The conclusions are the same regardless of the particle type. As expected, the central section A presents the best detection efficiency while section D, which is located at the corner of the neutron monitor, presents the worst one. The detection efficiency of sections B and C is somewhere in between, with section B presenting a little better efficiency.

All the previous simulations correspond to vertical incident directions. However, a particle may hit the neutron monitor in any angle. In order to examine how the direction of the incident particle affects the detection efficiency, the neutron monitor is rotated in a specific angle related to plane X–Z and the counts that it measures are recorded. The simulations were performed for neutron, proton and  $\pi^\pm$  particle beams (perpendicular to X–Z plane) and for energies from 100 MeV to 100 GeV. The angles that were simulated were the 15°, 30°, 45°, 60°, 75°, 80°, 85° and 90° in two azimuth cases 0° and 90°. Azimuth 0° corresponds to rotation of the NM around the Z axis (across the counters) while azimuth 90° corresponds to rotation around the X axis (along the counters). This set of simulations was the most time consuming since all the particle types were combined with all the angle cases for all the energy values. The simulation time was also increased due to the fact that each case was repeated 20 times in order for the statistical accuracy to be achieved. The mean counts per incident particle in respect to the energy and the incident direction are presented in 3D plots format in Fig. 10. As it can be seen the results

are identical for all the particle types, and the only change is that the counts for neutrons and protons are greater than in the case of pions. For the case of azimuth 0°, it is noticed that the efficiency increases with the increase of incident angle. The increase is more significant in high energies. The reason of this phenomenon is that the increase of the angle also increases the path of the particles into the NM and as a result more interactions take place. A different conclusion comes out in the case of azimuth 90°. In this case, the detection efficiency increases up to 85° and then there is a decrease. The reason for this is that in azimuth 90°, as the angle increases the beam becomes parallel with the counters. When the beam is completely parallel with the counters (at 90° angle), many incident particles do not pass through the producer but pass through the counters without any interaction.

### 6. Produced neutrons and energy spectrum

As it has already been mentioned, the operation of the neutron monitor is dominated by the generations of the secondary neutrons, their slowing down procedure to thermal energies and their capture in the counters. The number of the produced neutrons increases as the energy of the incident particle increases too. This effect is depicted in Fig. 11 where two screenshots of the simulation are showing the tracks of the produced neutrons (white lines) in the case of an incident neutron with energy 1 GeV and 100 GeV, respectively. The reflection of neutrons in the polyethylene reflector can also be noticed.

The number of generated neutrons, their capture in Boron-10 and the registered counts has been recorded in all the simulation runs of this work. For the case of a neutron beam in the vertical

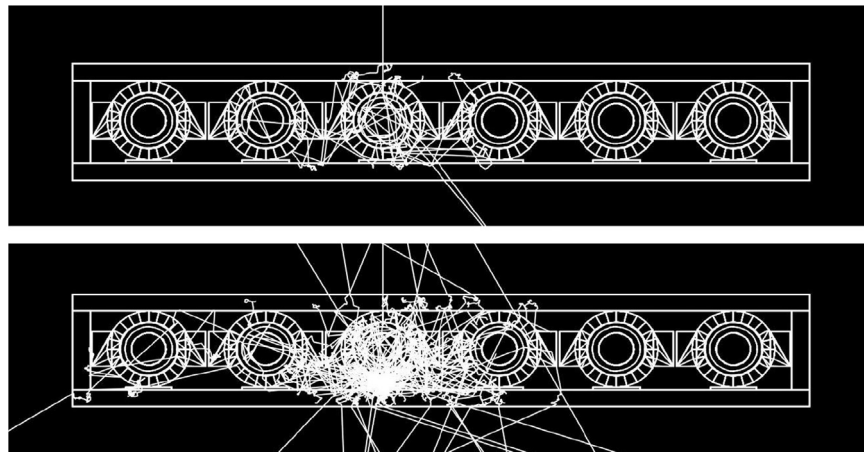


Fig. 11. Typical example of the secondary neutrons production for 1 GeV (upper) and 100 GeV (bottom) energy.

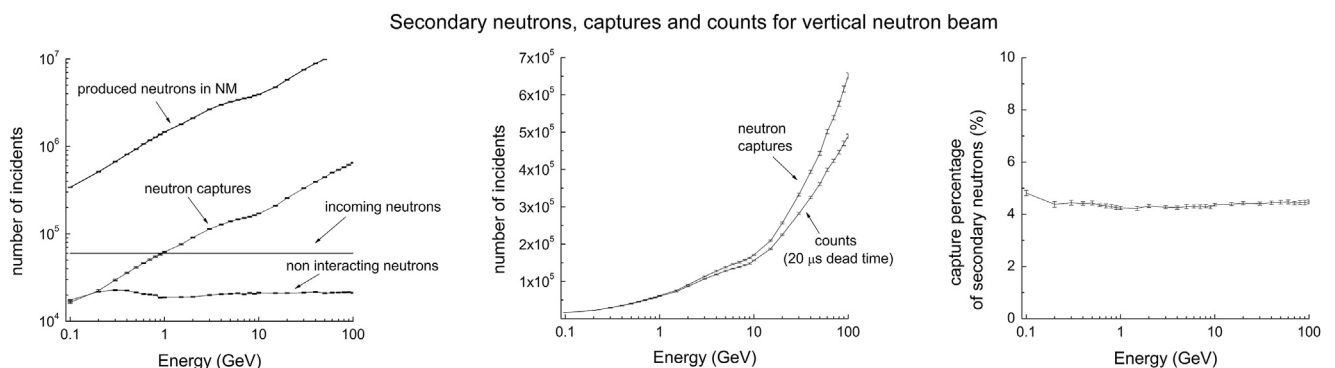


Fig. 12. Secondary neutrons and counts (left), relation of neutron captures and counts for 20  $\mu$ s dead time (center) and percentage of secondary neutrons capture (right) for vertical neutron beam.

direction, Fig. 12 shows some important parameters about the secondary neutrons. Referring to the left plot, it is noticed that about one third of the neutrons that enter the neutron monitor do not interact at all and this portion is independent of the energy. The neutrons that finally interact, initiate a cascade of secondary neutrons. The number of secondary neutrons increases as the energy increases, however, only 4.5–5% of them is finally captured in the counters, as it can be seen on the right plot. The central plot finally, shows the relation between the captures that take place in the counters and the counts that are registered. The difference is due to the fact that the electronic system of the neutron monitor has a dead time. As a result some of the neutron captures cannot be registered because another registration process is in progress. The standard dead time for the counters of the 6NM-64 (BP-28 counters) is 20  $\mu$ s and considering this value, it is noticed that up to 2 GeV almost all the neutron captures are registered as counts. From this energy and up, the number of captures is greater than the number that the acquisition system can measure. At this point it should be highlighted that some stations have technically increased the dead time in order to increase the sensitivity of the neutron monitor in low energies.

Finally, the energy of the secondary neutrons for vertical neutron beams with energy 0.1 GeV, 1 GeV, 10 GeV, 40 GeV, 70 GeV and 100 GeV are presented in Fig. 13. It is noticed that the histograms for all cases are identical and only the total number of neutrons is changed, as expected. The analysis of the spectrum shows that there is a smooth energy peak at about 500 keV. Additionally, there are also three distinct energy peaks. The first peak is a huge one and is located at the beginning of the histograms, which means that it corresponds to thermal neutrons,

while the other two are smaller and are located at about 100 keV and 418 keV.

## 7. Conclusion

A complete simulation analysis on the operation of the 6NM-64 neutron monitor was performed using Geant4. This type of neutron monitor is the one that Carmichael had standardized in the past and is still being operated from many cosmic ray stations, including the Athens Station. The analysis showed that the neutron monitor is sensitive in the hadronic component of the cosmic rays while the detection efficiency is slightly better for neutrons and protons than for pions, for energies above 100 MeV. For energies below 100 MeV, the role of the reflector is significant. A study on the detection efficiency of the different surface sections of the neutron monitor showed that there is a large central region in which the efficiency does not change significantly. Also, the detection efficiency is increased as the angle between the vertical and the incident direction increases. An exception is the case where the tracks of the incident particles are parallel to the counters. In this case a reduction of the efficiency is noticed.

Finally, a study was performed on the generations and the capture of the secondary neutrons. The results showed that although one third of the incident particles do not interact with the neutron monitor, a great number of secondary neutrons is produced. The number of secondary neutrons increases with energy, however only the 4.5–5% are captured in the counters. The dead time of the electronics reduces the measured counts comparing to the captures. For a dead time of 20  $\mu$ s, which is the

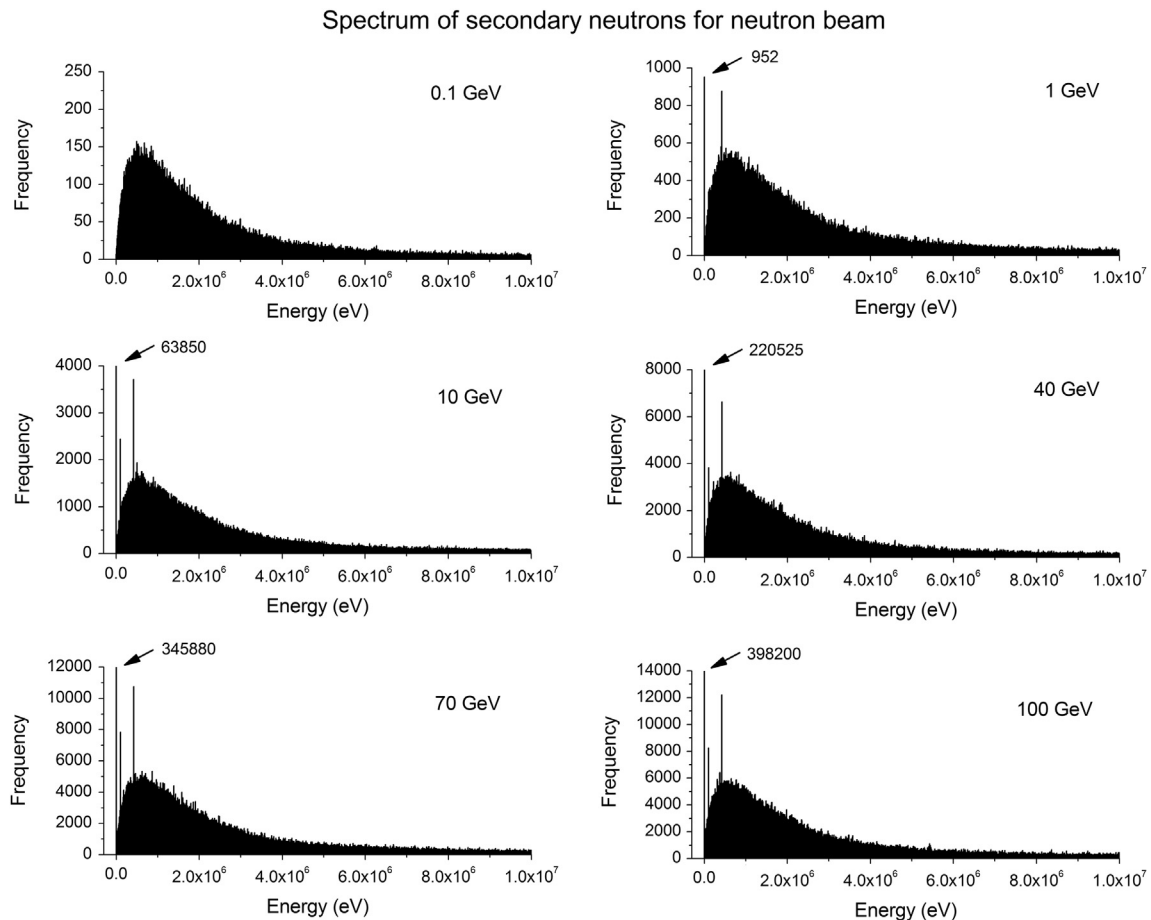


Fig. 13. Spectrum of produced neutrons into the 6NM-64 for several energies of vertical neutron beam.

standard for the electronics of 6NM-64, a difference between the captures and the counts is noticed above 2 GeV.

### Acknowledgments

Thanks are due to all the colleagues from the Neutron Monitor stations kindly providing their cosmic ray data. Athens Neutron Monitor station is supported by the Special Research Account of Athens University. The research leading to these results has received funding from the European Community's Seventh Framework Programme (FP7/2007-2013) NMDB under grant agreement No. 213007.

One of us (LID) thanks Israeli Ministry of Science for support in the frame of the project "National Centre of Knowledge in Cosmic Rays and Space Weather".

Thanks are also due to Dr. John Apostolakis for his important advices and discussions about Geant4 toolkit and to Dr. Dimitrios Tsirigkas for his valuable help in the simulation runs. Finally many thanks to the anonymous referee for your valuable comments improving this manuscript.

### References

- [1] J.A. Simpson, Cosmic Radiation Neutron Intensity Monitor, *Annals of the Int. Geophysical Year IV*, Pergamon Press, London (1958) 351. (Part VII).
- [2] H. Carmichael, *IQSY Instruction Manual*, Deep River, Canada, 1964.
- [3] C.J. Hatton, *The Neutron Monitor, Progress in Elementary Particle and Cosmic-ray Physics*, North Holland Publishing Co., Amsterdam, 1971. (chapter 1).
- [4] Mavromichalaki, H. et al., Athens neutron monitor and its aspects in the cosmic-ray variations studies. In: *Proceedings of 27th ICRC 2001 Hamburg*, 10, 4099–4103, 2001.
- [5] P.H. Stoker, L.I. Dorman, J.M. Clem, *Space Science Review* 93 (2000) 361.
- [6] M. Storini, F. Signoretti, P. Diego, F. Re, M. Laurenza, *Advances in Space Research* 43 (2009) 721.
- [7] F. Signoretti, M. Storini, *Astrophysics and Space Sciences Transactions* 7 (2011) 11.
- [8] S. Semikh, S. Serre, J.-L. Aufran, D. Munteanu, S. Sauze, E. Yakushev, S. Rozov, *IEEE Transactions on Nuclear Science NS59* (2) (2012) 303.
- [9] H. Mavromichalaki, *World-wide Integration of Neutron Monitors–The NMDB Project*, EOS AGU (2010) 305–306. (2010).
- [10] H. Mavromichalaki, et al., *Advances in Space Research* 47 (2011) 2210.
- [11] J.A. Simpson, *Space Science Reviews* 93 (2000) 1.
- [12] J.M. Clem, L.I. Dorman, *Space Science Reviews* 93 (2000) 335.
- [13] H. Mavromichalaki, et al., *Annales Geophysicae* 23 (2005) 3103.
- [14] H. Mavromichalaki, et al., *Advances in Space Research* 44 (2009) 1237.
- [15] S. Agostinelli, et al., *Nuclear Instruments and Methods in Physics Research Section A: Accelerators, Spectrometers, Detectors and Associated Equipment* 506 (3) (2003) 250.
- [16] J. Allison, et al., *IEEE Transactions on Nuclear Science NS53* (1) (2006) 270.
- [17] Banerjee S. et al., *Detector Description of CMS Using Geant4*, CMS Note, 1999.
- [18] Costanzo D. et al., *The Geant4-based simulation software of the ATLAS detector*, in: *Nuclear Science Symposium Conference Record, IEEE*, , 1, 5–11, 2006.
- [19] J. Apostolakis, et al., *Journal of Physics: Conference Series* 119 (2008) 032004.
- [20] A. Schaelicke, et al., *Journal of Physics: Conference Series* 331 (2011) 032029.
- [21] Planetocosmics, <http://cosray.unibe.ch/~laurent/planetocosmics>.
- [22] Magnetocosmics, <http://cosray.unibe.ch/~laurent/magnetocosmics>.
- [23] Yu.V. Balabin, B.B. Gvozdevskij, E.A. Maurchev, E.V. Vashenyuk, D.D. Dzhappuev, *Astrophysics and Space Sciences Transactions* 7 (2011) 283.
- [24] E.A. Maurchev, B.B. Gvozdevskij, J.V. Balabin, E.V. Vashenjuk, *Modellig of Hadron Interactions in the Neutron Monitor, Physics of Auroral Phenomena, Proceedings of the XXXIII Annual Seminar* (2011) 83. (Apatity).
- [25] Shibata S. et al., *Nuclear Instruments and Methods in Physics Research Section A: Accelerators, Spectrometers, Detectors and Associated Equipment*, 463, 316–320, 2001.